PD-1-induced T cell exhaustion is controlled by a Drp1-dependent mechanism

Luca Simula[1], Valeria Cancila[2], Ylenia Antonucci[1], Alessandra Colamatteo[3], Claudio Procaccini[4,5], Giuseppe Matarese[3,4], Claudio Tripodo[2,6], and Silvia Campello[1,*]

[1]*Department of Biology, University of Rome Tor Vergata, Rome, Italy*
[2]*Tumor Immunology Unit, Department of Health Sciences, University of Palermo School of Medicine, Italy*
[3]*Department of Molecular Medicine and Medical Biotechnologies, University of Naples Federico II, Naples, Italy*
[4]*Institute for Endocrinology and Experimental Oncology "G. Salvatore", CNR, Naples, Italy*
[5]*IRCCS Santa Lucia Foundation, Rome, Italy*
[6]*Histopathology Unit, FIRC Institute of Molecular Oncology (IFOM), Milan, Italy*

[*]*corresponding author:* silvia.campello@uniroma2.it

Abstract

PD-1 signalling downregulates the T cell response, promoting an exhausted state in tumor-infiltrating T cells, through mostly unveiled molecular mechanisms. Drp1-dependent mitochondrial fission plays a crucial role to sustain T cell motility, proliferation, survival and glycolytic engagement and, interestingly, such processes are exactly those inhibited by PD-1 in tumor-infiltrating T cells. Here we show that PD1^{positive} CD8+ T cells infiltrating MC38-derived murine tumor mass show downregulated Drp1 activity and more fused mitochondria compared to PD1^{negative} counterparts. Also, PD1^{positive} lymphocytic elements infiltrating human colon cancer almost never express active Drp1. Mechanistically, PD-1 signaling directly prevents mitochondria fragmentation following T cell stimulation by downregulating Drp1 phosphorylation on Ser616, via regulation of the ERK1/2 pathway and, to a lesser extent, of mTOR. In addition, downregulation of Drp1 activity in tumor-infiltrating PD1^{positive} CD8+ T cells seems to be a mechanism exploited by PD-1 signaling to reduce motility and proliferation of these cells. Overall, our data indicate that the modulation of Drp1 activity in tumor-infiltrating T cells may become a valuable target to ameliorate the anti-cancer immune response in future immunotherapy approaches.

Keywords: Drp1, mitochondria, PD-1, T cell, tumor-infiltrating lymphocytes, mitochondrial dynamics, cell migration

INTRODUCTION

Programmed Cell Death-1 (PD-1) is a T cell surface receptor that down-regulates T cell activation and the immune response (1). PD-1 signaling is activated by PD-1 interaction with its ligands PD-L1 and PD-L2, expressed on adjacent cells (2), and it dampens signals originating from T Cell Receptor (TCR) and CD28, such as the activation of mammalian-Target-of-Rapamycin (mTOR) and Mitogen-Activated-Protein-Kinases (MAPK) pathways (3, 4). Besides being frequently observed in T cells during chronic infections (5), activation of PD-1 signaling has also been widely reported in tumor-infiltrating T cells, contributing to their functional exhaustion and poor anti-tumor response (6). Consistently, antibodies targeting the interaction between PD-1 and its ligands efficiently reinvigorate tumor-infiltrating T cells, thereby ameliorating anti-tumor response (7, 8). On the other side, impaired PD-1 function plays an important role in a variety of autoimmune diseases (9).

Mitochondria are central modulators of cellular bioenergetics, and their dynamic morphology (i.e. a fragmented or fused network) is tightly linked to cell functions (10). Among the mitochondria-shaping proteins, Mitofusin-1 and -2 (Mfn1 and Mfn2) and Optic-Athropy-1 (Opa1) are the main regulators of mitochondria fusion (11, 12), while Dynamin-Related Protein-1 (Drp1) is the main pro-fission protein and it is recruited from the cytosol to mitochondria thanks to several receptors, such as Mff and Fis1 (13, 14). These mitochondria-shaping proteins are regulated at both transcriptional and post-translational levels (10).

Interestingly, mitochondria morphology is tightly linked to an optimal T cell functionality. Particularly, Drp1-dependent mitochondria fragmentation sustains T cell motility and proliferation (15), and effector T (T_{eff}) cell apoptosis following TCR engagement (16). Also, Drp1-dependent mitochondria relocation at the immunological synapse controls the influx of calcium upon T cell activation (17), sustaining the cMyc-dependent upregulation of glycolytic enzymes (15, 18), thus allowing the metabolic reprogramming required to cope with the increased bioenergetic demand of an activated T cell (19, 20). All these processes contribute to an optimal anti-tumor T cell response, which is indeed defective in T cells lacking Drp1 (15).

Of note, most of those Drp1-dependent processes are the same that appear to be down-regulated by PD-1 inhibitory signaling, especially when considering tumor-infiltrating T cells. Indeed, PD-1 signaling reduces T cell proliferation and motility (both of them requiring Drp1) (4, 15, 21), and it also promotes a shift from a glycolysis-based metabolism (supported by Drp1) toward an OXPHOS-based metabolism (requiring mitochondrial fusion) (22). Given this striking inverse correlation, we asked whether PD-1 signaling may modulate Drp1 activity, and to what extent this modulation may down-regulate several processes in T cells. This point is of extreme importance, since the molecular mechanisms by which PD-1 regulates the aforementioned processes in T cells are not yet completely understood.

We here show that tumor-derived PD-$1^{positive}$ CD8+ T cells exhibit a significant down-regulation of Drp1 activity and a more fused mitochondrial network. Mechanistically, PD-1 signaling prevents Drp1 activation following T cell stimulation by regulating its phosphorylation on Ser616 through the modulation of Extracellular-Regulated Kinase 1/2 (ERK1/2) proteins. Also, we provide evidence that Drp1 down-regulation contributes to the reduced proliferation and motility of PD-$1^{positive}$ tumor-infiltrating T cells and, as a consequence, identify Drp1 as a possible target for future therapeutic approaches aiming at restoring anti-tumor response in $PD1^{positive}$ exhausted CD8+ T cells.

RESULTS

PD1^{positive} CD8+ T cells from MC38-derived murine tumors show a reduced mitochondrial fission.

To investigate if PD1 signaling modulated the morphology of the mitochondrial network, we decided to look at PD1^{negative} (PD1^{neg}) and PD1^{positive} (PD1^{pos}) CD8+ T cells infiltrating a 18 days-old solid tumor mass derived from s.c. inoculation of MC38 cells (murine adenocarcinoma) in c57BL/6 WT mice. We decided to take advantage of this tumor model, since we previously reported it as being characterized by a high level of T cell infiltration (15). By comparing expression levels of different mitochondria-shaping proteins in infiltrating CD8+ T cells (TILs) by intracellular flow cytometry, we observed that PD1^{pos} CD8+ TILs show a specific down-regulation of Drp1 phosphorylation on its activating residue Ser616 (**Fig. 1A**) compared to PD1^{neg} CD8+ TILs, while total Drp1 levels and the inhibitory phosphorylation on Ser637 did not vary (**Fig. 1A**). Also, we did not observe any differences in the expression of other main pro-fusion (Mfn1, Mfn2, Opa1) or pro-fission (Fis1, Mff) proteins (**Fig. 1A**).

Consistently, such a reduction in active Drp1 levels in PD1^{pos} CD8+ TILs correlates with an altered morphology of mitochondria. In fact, we found that sorted PD1^{pos} CD8+ TILs show a tendency toward a more fused mitochondrial network when compared to PD1^{neg} CD8+ TILs (**Fig. 1B** and **Supplemental Figure S1**). Interestingly, this is observed even if sorted CD8+ TILs were stimulated for 2h with beads coated with anti-CD3/28 Abs plus PD-L1 (PD-1 ligand) before fixation (**Fig. 1C**), suggesting that such a fusion-prone mitochondria morphology may also influence T cell activation upon antigen encounter in a PD-L1-rich environment (such as a tumor mass).

Last, we extended these observations to a corresponding human tumor context, by staining sections of human colon carcinoma moderately differentiated (G2) cases with anti-PD-1 and anti-Drp1-pSer616 antibodies. Of note, we found that tumor-infiltrating lymphocyte elements almost never co-express PD-1 and active Drp1 (indeed, only less than 5% of cases were double positive) (**Fig. 1D**), with this suggesting that also in a human tumor context PD1^{pos} T cells downregulate Drp1 activity.

In sum, tumor-infiltrating PD1^{pos} CD8+ T cells show a tendency toward a more fused mitochondria morphology, associated with a reduced activation of Drp1.

PD1 signaling prevents Drp1 activation and mitochondria fragmentation in both murine and human T cells, upon *in vitro* stimulation.

To investigate whether such altered Drp1 expression in PD1^{pos} CD8+ TILs is directly caused by PD-1 activation, we switched to an *in vitro* system to specifically modulate PD-1 signaling. To this aim, we stimulated *in vitro* T cells isolated from spleen of WT mice with beads coated with anti-CD3/28 plus BSA (thereafter aCD3/28-beads) or anti-CD3/28 Abs plus PD-L1 (thereafter aCD3/28-PDL1-beads) for 48h. As expected, concomitant activation of PD-L1/PD-1 axis during T cell stimulation dampens activation of both mTOR and ERK1/2 pathways (as assessed by monitoring the corresponding activating phosphorylated residues) (**Fig. 2A**) (3, 4). Interestingly, we also observed that Drp1 phosphorylation on Ser616 (activating residue) is strongly reduced by the engagement of PD-1 signaling (**Fig. 2A**), while no significant differences were observed for other mitochondria-shaping proteins (**Fig. 2B**). In line with this, while T cells fragment mitochondria upon activation (15, 16, 23), T cells stimulated in the presence of PD-L1 retain a more fused

network (**Fig. 2C**). Of note, mitochondria of murine activated T cells might characteristically appear slightly swollen when fragmented (**Fig. 2C**), still being fully functional (**Supplemental Figure 2A-B**).

In addition, such an absence of fragmented mitochondria in PD-L1-stimulated T cells is not due to ongoing mitophagy (which could hypothetically promote the clearance of the small and fragmented mitochondria). Indeed, we did not observe any significant sign of mitophagy (by checking MnSOD levels) in T cells stimulated with either aCD3/28- or aCD3/28-PDL1-beads (**Supplemental Figure S2C**), although autophagy is normally active.

Last, a PD-1-dependent Drp1 modulation was also observed in human T cells isolated from peripheral blood (hPBT). Similar to their murine counterpart, hPBT cells stimulated for 48h with aCD3/28-PDL1-beads do not show Drp1 phosphorylation on Ser616 (**Fig. 2D**) and do not fragment their mitochondria upon activation (**Fig. 2E**) at the same level as hPBT cells stimulated with aCD3/28-beads, which also display higher mTOR and ERK1/2 activation (**Fig. 2D**).

These data indicate that co-stimulation of PD-1 signaling during T cell activation prevents Drp1 phosphorylation and mitochondria fragmentation both in mice and human.

Both naïve and memory murine CD8+ T cells show reduced Drp1-dependent mitochondria fragmentation upon engagement of PD1 signaling during activation.

Next, we decided to look more closely at naïve (T_{nv}) and memory (T_{mem}) CD8+ T cell subpopulations, which, once activated, may undergo exhaustion within the tumor microenvironment. Of note, although naïve CD8+ T cells do not express PD-1 on their cell surface, they rapidly acquire PD-1 expression after 12h stimulation with aCD3/28-beads (as also observed for naïve CD4+ T cells), and the concomitant presence of PD-L1 ligand does not affect such upregulation (**Supplemental Figure S3A**). We thus isolated both subpopulations from the spleen of WT mice and stimulated them *in vitro* with aCD3/28- or aCD3/28-PDL1-beads for 48h, which is the optimal time point to detect Drp1 phosphorylation, especially in naïve CD8+ T cells (**Supplemental Figure S3B**). Interestingly, we found that engagement of PD-1 signaling during activation dampens Drp1 phosphorylation and mitochondria fragmentation in both CD8+ T_{nv} and T_{mem} cells (Fig. 3A-B), in parallel with a reduced activation of ERK and mTOR pathways (**Fig. 3A**).

Activation of PD-1 signaling is one of the hallmarks of exhausted T cells. Our *in vitro* observation that the engagement of PD-1 signaling prevents Drp1 phosphorylation and mitochondria fragmentation (see Figs. 2-3) is consistent with our data *in vivo*, indicating that $PD1^{pos}$ (exhausted) CD8+ TILs show reduced Drp1 activity and more fused mitochondria (see Fig. 1). *In vivo*, $PD1^{pos}$ (exhausted) CD8+ TILs may also arise through repetitive cycles of TCR stimulation. Therefore, to investigate whether Drp1 downregulation correlates with PD1 upregulation also in this case, we took advantage of an alternative *in vitro* system to induce an exhausted-like state in CD8+ T cells. Indeed, subsequent cycles of *in vitro* stimulation of naïve CD8+ T cells (up to 4 stimulation for 24h, each one followed by 6 days in IL2-containing medium) induce a functional exhausted-like state characterized by diminished cytokine production, proliferative capacity, and cytotoxic potential (24). Of note, we previously reported that such protocol *in vitro* induces a robust and progressive PD-1 upregulation in CD8+ T cells (increasing its expression further at each stimulation), and eventually mimicking the $PD1^{pos}$ exhausted-like state of tumor-engaged T cells (15). Interestingly, we observed that upon subsequent cycles of naïve CD8+ T cell stimulation, the

level of Drp1 phosphorylation on Ser616 progressively decreases (**Fig. 3C**), in line with a progressively less fragmented morphology of the mitochondria (**Fig. 3D**). Therefore, increasing PD-1 expression in CD8+ naïve T cells upon multiple *in vitro* stimulations correlates with a progressive inhibition of the ability of these cells to fragment mitochondria.

In sum, these data indicate that PD-1 signaling prevents Drp1-dependent mitochondria fragmentation in both naïve and memory murine CD8+ T cells. Also, impaired Drp1 activity is observed in *in vitro*-induced exhausted-like CD8+ T cells, too.

PD1 signaling downregulates Drp1 activation by modulating mTOR and ERK pathways.

Next, we decided to better investigate the molecular pathways linking PD-1 activation to downregulation of Drp1 activity. PD-1 signaling dampens both PI3K/Akt/mTOR pathway downstream of CD28 activation (3) and MAPK/ERK pathway downstream of TCR engagement (4), as indeed confirmed by our results (see **Fig. 2A, D**). Of note, both these pathways have been reported to modulate Drp1-dependent mitochondria fragmentation. Indeed, ERK1/2 directly phosphorylate Drp1 on Ser616 (25), as we already showed in T cells, too (15, 16, 26). Similarly, the mTOR pathway promotes mitochondria fragmentation via Drp1 activation (27), even though it is supposed to not directly phosphorylate Drp1, and rather acting through the modulation of ERK activity, as suggested in murine embryonic fibroblasts (27). Also, mTOR and ERK pathways extensively crosstalk and support each other (28, 29). Therefore, our working hypothesis is that concomitant activation of PD-1 signaling upon T cell stimulation dampens both mTOR and ERK pathways, these being required for Drp1 phosphorylation on Ser616.

To test this hypothesis, we first activated murine T cells in the presence of mTOR inhibitor RAD-001 (30), and observed that RAD-001 prevents both mTOR auto-phosphorylation and ERK phosphorylation (**Fig. 4A**). Also, it reduces Drp1 phosphorylation on Ser616 and mitochondria fragmentation (**Fig. 4A-B**). Second, we have reported previously that ERK1/2 inhibitor FR180204 (ERKi) prevents Drp1 phosphorylation upon both chemokine stimulation and TCR engagement in T cells (31), and further confirmed the latter condition here again (**Fig. 4C**). Also, ERKi prevents mitochondria fragmentation upon T cell activation (**Fig. 4D**). Therefore, inhibition of mTOR and ERK pathways (as observed upon activation of PD-1 signaling) impacts Drp1 activity and mitochondria fragmentation upon activation. Last, to confirm that ERK1/2 proteins, which are inhibited by PD-1 pathways, are the kinases directly responsible for Drp1 modulation, we rescued ERK1/2 activity downstream of PD-1 signaling. To this aim, we activated hPBT cells with aCD3/28- or aCD3/28-PDL1-beads in presence of low doses of C6-ceramide (to avoid apoptosis induction), a known activator of the ERK pathway (32). Of note, ceramide, which slightly increase ERK phosphorylation, rescues Drp1 phosphorylation on Ser616 and mitochondria fragmentation in PD-1-engaged T cells during activation (**Fig. 4E-F**).

In sum, activation of PD-1 signaling during T cell stimulation reduces Drp1 phosphorylation and mitochondria fragmentation through direct inhibition of the ERK pathway, and concomitant dampening of mTOR activity. The latter may support indirectly Drp1-dependent mitochondria fragmentation by sustaining the ERK pathway, even though there is the possibility that it could also modulate Drp1 independently from ERK.

Drp1 is required for an efficient reduction of tumor growth mediated by anti-PD-1 therapy.

Most processes downregulated by PD-1 inhibitory signaling in T cells (proliferation, motility, glycolytic engagement) are the same requiring Drp1 to function correctly (4, 15, 21). Therefore, we asked to what extent PD-1 signaling may down-regulate such processes in T cells via inhibition of Drp1 activity, especially in cancer. To answer this point, we analysed the s.c. growth of MC38-derived tumors in WT mice, which can be significantly reduced by treatment with anti-PD-1 Ab, also increasing the amount of infiltrating leukocytes (33). Also, we previously reported that MC38-derived tumors growth faster in mice lacking Drp1 specifically in T cells (15). Therefore, we s.c. inoculated MC38 cells into both control ($Drp1^{fl/fl}$) and Drp1 conditional-KO ($Drp1^{fl/fl}$Lck:cre+, T cell-restricted Drp1 ablation, indicated as Drp1cKO) mice. After one week, we treated these mice with either anti-IgG (control) or anti-PD-1 Ab every 2/3 days for up to 10 days (**Fig. 5A**). Of note, we found that anti-PD-1 treatment is much more efficient in reducing tumor growth in control mice than in mice where Drp1 was absent from T cells (Drp1-cKO) (**Fig. 5B**). Since Drp1 ablation in T cells favors *per se* a faster tumor growth in this model (15), we also compared the relative percentage of reduction in tumor growth (anti-PD-1 / anti-IgG ratio) to correct for the larger tumor volume in Drp1-cKO mice compared to control mice. Even so, we still observed that while anti-PD-1 treatment reduces tumor growth by ca. 60% in control mice, this percentage drops to just ca. 20% in Drp1-cKO ones (**Fig. 5C**). In addition, we found that in control ($Drp1^{fl/fl}$) mice, where Drp1 phosphorylation is reduced in $PD1^{pos}$ CD8+ TILs when compared with $PD1^{neg}$ TILs, anti-PD-1 treatment is able to increase and restore Drp1 phosphorylation in $PD1^{pos}$ CD8+ T cells to a level comparable to $PD1^{neg}$ CD8+ T cells (**Fig. 5D**).

Therefore, anti-PD-1 treatment restores Drp1 phosphorylation on Ser616 in control CD8+ TILs and this correlates with a significant reduction in tumor growth. On the contrary, in Drp1-cKO mice (where Drp1 is absent and therefore cannot be "rescued" by anti-PD-1 treatment), anti-PD-1 treatment is much less efficient in reducing tumor growth. Overall, these data suggest that, among the processes restored by anti-PD-1 treatment in CD8+ exhausted TILs, at least some of them requires a functional Drp1 (and are therefore not rescued in Drp1-cKO mice) and, consequently, that the mechanisms by which PD-1 signaling inhibits T cell activity may require Drp1 inhibition at least for some of the processes involved.

Next, we decided to get more insight into such processes mediated by Drp1 downregulation downstream of PD-1 signaling. Of note, while anti-PD-1 treatment increases the number of CD8+ TILs recovered from the tumor mass (per mm^3), this effect is not observed in Drp1-cKO mice (**Fig. 5E**), indicating that Drp1 is required to mediate such anti-PD-1-dependent increase in CD8+ TILs accumulation. Although Drp1 is required to sustain IFNγ production in CD8+ TILs (15), this does not seem to be related to the impaired accumulation of Drp1-KO CD8+ TILs after anti-PD-1 treatment. Indeed, upon anti-PD-1 treatment, Drp1-KO CD8+ TILs increase IFNγ production to a level similar to control CD8+ TILs (**Fig. 5F**), suggesting that PD-1-dependent regulation of IFNγ production does not involve Drp1. We previously reported that Drp1 is also required to sustain T cell clonal expansion after stimulation, both *in vitro* and *in vivo* (15). Therefore, we asked whether the inability of Drp1-KO CD8+ TILs to increase their number within the tumor mass upon anti-PD-1 treatment may depend or not on their impaired proliferation. To this aim, we isolated TILs from MC38-derived tumor masses grown in control or Drp1-cKO mice (treated with anti-IgG or anti-PD-1) and let them expand *in vitro* in the presence of IL-2, IL-7 and IL-15 cytokines. Interestingly, while the anti-PD-1 treatment significantly increases fold expansion of control CD8+ T cells, this effect is completely lost in Drp1-KO CD8+ T cells (**Fig. 5G**). These data suggest that Drp1

inhibition may be at least one of the mechanisms by which PD-1 signaling reduces proliferation of $PD1^{pos}$ CD8+ TILs.

In sum, a functional Drp1 is required for the efficacy of the anti-PD-1 treatment in reducing MC38-derived tumor growth in mice. Also, PD-1 signaling may mediate the reduction in CD8+ TILs proliferative potential via Drp1 downregulation.

Reduced motility of $PD1^{pos}$ and *in vitro* exhausted-like T cells correlates with altered Drp1-dependent mitochondria remodeling.

Besides controlling T cell proliferation, Drp1 is required to sustain T cell motility by favoring mitochondria repositioning at the uropod and it is directly phosphorylated on Ser616 in response to chemokine stimulation (15, 34). Also, T cell motility is another process dampened by PD-1 signaling (21). Therefore, in addition to controlling proliferation of $PD1^{pos}$ CD8+ TILs, the PD-1-dependent downregulation of Drp1 activity may also account for their reduced motility. To address this point, we isolated TILs from MC38-derived tumor masses grown in control or Drp1-cKO mice (treated with anti-IgG or anti-PD-1) and let them starve from serum *in vitro*. Then, we assayed their migratory ability in response to serum by using the transwell migration assay. Interestingly, we found that anti-PD-1 treatment significantly increases motility of control $PD1^{pos}$ CD8+ TILs, when compared to the motility of the same cells from anti-IgG-treated control mice (**Fig. 6A**), while it does not improve the motility of $PD1^{neg}$ CD8+ T cells, as expected (**Fig. 6A**). However, this effect is completely lost when looking at $PD1^{pos}$ CD8+ TILs from Drp1-cKO mice, whose T cells lack Drp1 (**Fig. 6A**). These data suggest that Drp1 inhibition may be one of the mechanisms by which PD-1 signaling reduces motility of $PD1^{pos}$ CD8+ TILs.

To analyze in more details the modulation of Drp1 in functional and exhausted T cells during T cell migration, we switched to our *in vitro* model to induce an exhaustion-like state in CD8+ T cells (as already described in **Fig. 3C-D**). We thus compared the migratory ability of effector (T_{eff}) CD8+ T cells (stimulated only once) and exhausted-like (T_{ex}) CD8+ T cells (stimulated 4 times). As expected, T_{ex} cells migrate much less than T_{eff} cells (**Fig. 6B**). Interestingly, we also observed that while functional T_{eff} cells correctly polarize the mitochondria at the uropod (**Fig. 6C**), a process requiring Drp1 (15), and show both Drp1 and ERK1/2 phosphorylation upon chemokine stimulation (**Fig. 6D**), in T_{ex} cells the mitochondrial network fails to rearrange (Fig. 6C), and Drp1 and ERK1/2 are unresponsive to chemokine stimulation (**Fig. 6D**), this implying the lack of key steps normally required for T cell motility.

Overall, these data indicate that PD-1 signaling may mediate the reduction in CD8+ TILs motility via Drp1 downregulation. Also, *in vitro*-induced exhausted-like T cells are unable to respond to chemokine stimulation by activating Drp1 and by rearranging their mitochondrial network, this providing a mechanistic basis for their impaired motility.

DISCUSSION

It has been reported that tumor-infiltrating T cell show altered mitochondria functionality and morphology when compared with T cells from peripheral blood (35). However, modulation of mitochondria morphology in different subpopulation of TILs (such as $PD1^{pos}$ and $PD1^{neg}$ cells) has never been investigated before. We here report that $PD1^{pos}$ MC38-derived tumor-infiltrating murine CD8+ T cells display an altered mitochondria morphology when compared with $PD1^{neg}$ counterparts. Indeed, they are characterized by a reduced Drp1 activation and a more fused morphology of mitochondria. Of note, these data are shared also in a corresponding human context of colon tumor, in which tumor-infiltrating lymphocytic elements almost never co-express PD-1 and active Drp1. Mechanistically, we provided evidence that PD-1 signaling downregulates Drp1 activating phosphorylation on Ser616 (and consequently mitochondria fragmentation) via the inhibition of ERK1/2 kinases, which directly phosphorylate Drp1 on this residue (15, 16, 25). Also, our data indicate that concomitant PD-1-dependent inhibition of mTOR pathway contributes to such a reduced Drp1 activity. This occurs presumably through mTOR ability to support the ERK pathway, as suggested before (27), even though we cannot exclude that mTOR may modulate Drp1 independently from its role on ERK.

Also, we explored the functional consequences of such PD-1-dependent downregulation of Drp1 activity in a tumor context. Of the highest importance, altogether, our data suggest that PD-1 signaling may exploit the downregulation of Drp1 activity to dampen some of the processes required for an optimal T cell functionality. Specifically, Drp1 downregulation seems to be involved in the inhibition of motility and proliferation of $PD1^{pos}$ CD8+ TILs. Indeed, anti-PD-1 treatment in mice fails to restore motility and proliferation of $PD1^{pos}$ CD8+ TILs (as it should), when Drp1 is not present in these cells (and therefore cannot be re-activated). Of note, we observed that the Drp1-dependent mitochondria relocation at the cell rear edge during cell migration (a phenomenon reported to occur in healthy effector CD8+ T cells) is completely lost in exhausted CD8+ T cells, which are unable to activate Drp1 upon chemokine stimulation. Our data are thus consistent with previous observations made in a persistent infection mouse model, in which the recovered motility of $PD1^{pos}$ T cells upon anti-PD-1 treatment were associated with an increased ERK activation (21). Indeed, we previously reported that, during T cell migration, ERK1/2 mediates Drp1 phosphorylation, which is then required to sustain T cell motility (15), and we here report that exhausted T cells fails to activate Drp1 and fragment mitochondria upon chemokine stimulation. Therefore, downregulation of ERK/Drp1 axis may be exploited by PD-1 signaling to dampen T cell motility. Regarding the role of Drp1 in T cell proliferation, we previously reported that, in the absence of Drp1, T cells show an abnormal length of mitosis, due to the acquisition of aberrant centrosome morphologies (15), as observed also in cancer cells (36).

In sum, our data indicate that downregulation of Drp1 mediated by PD-1 signaling may be required to attain an efficient inhibition of T cell response. Therefore, we dare to propose Drp1 as a therapeutic target to ameliorate exhausted T cell functionality during anti-cancer approaches, although drugs able to activate this protein need to be developed yet (26). Of note, CAR T cell-based approaches are currently being exploited for the treatment of solid cancers (37), but they frequently fail to confer long term tumor regression due to a poor ability of CAR T cells to survive and infiltrate within a solid tumor mass. This may be partially explained by the tendency of CAR T cells to undergo functional exhaustion, similar to endogenous T cells (38); however, whether or not a PD-1-dependent downregulation of Drp1 activity is present also in exhausted CAR T cells is still not known. Should such modulation be observed, targeting Drp1 activity in CAR T cells (either pharmacologically or genetically) could represent a new strategy to ameliorate CAR T cell survival (by increasing proliferation) or infiltration (by increasing motility).

In addition, although we here provided evidence that Drp1 downregulation may be exploited by PD-1 signaling to reduce tumor-infiltrating T cell motility and proliferation, other processes may be touched as well. First, we recently reported that Drp1 is required to allow cytochrome-c release and activation of caspases during the Activation-Induced Cell Death (AICD) progression in T cell following TCR engagement (16). Interestingly, T_{ex} cells require continuous engagement with antigen to persist long term (39), and this occurs in the absence of apoptosis induction, which normally takes place in short-lived T_{eff} cells via AICD. We are thus tempted to speculate that PD-1-dependent Drp1 downregulation in T_{ex} cells may also contribute to their long-term survival by reducing their tendency to undergo AICD. However, PD-1 signaling is also an apoptosis-inducer in T cell (40), this contributing to its inhibitory effect on T cell activation. Therefore, how exactly PD-1 and Drp1 correlate each other during T cell apoptosis is still not clear. Also, these data suggest that PD-1 signaling may regulate apoptosis in a Drp1- and mitochondria- independent way. Further studies will be required to shed light on this aspect.

Second, engagement of PD-1 signaling downregulates both glycolysis and OXPHOS in stimulated T cells (41). However, glycolysis is downregulated to a higher extent than OXPHOS, this forcing PD1-engaged T cells to rely more on an OXPHOS-based metabolism (22, 41). Although this mechanism may allow tumor-infiltrating T cells to survive in a tumor microenvironment characterized by low glucose availability (22), the underlying mechanism favoring such metabolic adaptation is not known yet. Ogando *et al.* recently reported that PD-1 signaling mediates disassembly of mitochondrial *cristae* (41). Since the *cristae* are required for an optimal OXPHOS-based metabolism (42), this observation may provide a putative mechanism by which PD-1 modulate the OXPHOS rate in T cells. This said, no clues are available about the mechanism by which PD-1 regulates glycolysis. Mitochondrial fragmentation is frequently associated with the engagement of a glycolytic metabolism, especially in cancer cells (10). This occurs in T cells, too. Indeed, upon T cell activation Drp1 sustains cMyc activation via a calcium/AMPK/mTOR axis (15), this in turn promoting upregulation of glycolytic enzymes and full activation of glycolysis (18). Also, Drp1-dependent mitochondria fragmentation reduces the functionality of the ETC complexes (43), further favoring an OXPHOS-to-glycolysis shift in T cell metabolism upon activation (44). Interestingly, we recently observed that Drp1-KO T cells show a glycolysis-to-OXPHOS metabolic shift upon activation, this explained by an increased FAO engagement and a reduced upregulation of cMyc-dependent glycolytic genes (15). Therefore, our observation that $PD1^{pos}$ CD8+ T cell downregulates Drp1 activation upon stimulation, besides contributing to their reduced proliferation and motility, may provide also a mechanistic basis for the downregulation of the glycolysis in these cells. Although further studies are required to firmly establish this point, we suggest the possibility that PD1 signaling could mediate the reduction of the glycolytic potential of CD8+ TILs at least partially via Drp1 downregulation.

Third, CD8+ TILs infiltrating human clear cell Renal Cell Carcinoma (ccRCC) were reported to show increased mitochondrial mass and ROS production (35). Drp1 may facilitate dismissal of small mitochondria via mitophagy (45). Interestingly, downregulation of Drp1 activity in $PD1^{pos}$ CD8+ TILs may provide a mechanism to reduce the mitophagy rate in these cells, preventing the generation of small mitochondria that can be targeted to degradation. This is consistent with the observation of a higher mitochondrial mass in CD8+ TILs (35).

Of note, Ogando *et al.* recently analysed the effect of PD-1 signaling on the assembly of mitochondrial *cristae* (41). Although they reported no variations in the rate of mitochondrial fragmentation in T cells stimulated in the presence or absence of PD-1 engagement, they also reported no differences in the rate of mitochondrial fragmentation between unstimulated and stimulated T cells (41). However, fragmentation of the mitochondrial network upon T cell

stimulation (independently of PD-1 signaling) has been reported extensively by us and others (15, 17, 23). We suppose that such discrepancy may rely partially on their use of the circularity as a parameter to estimate the rate of mitochondrial fragmentation upon T cell activation. Indeed, we believe that such a parameter may not be suitable to compare mitochondria morphology in stimulated and unstimulated naïve T cells, since the former cells grow and enlarge significantly compared to the latter ones upon *in vitro* culture. In addition, Ogando *et al.* only analysed total levels of Drp1, without focusing on its specific phosphorylated residues (41), which are more reliable indicators of Drp1 activation compared to the total protein amount.

To conclude, the modulation of Drp1 in tumor-derived exhausted T cells may represent a valuable target to ameliorate anti-cancer immune response in a number of instances and the manipulation of CAR T systems to this aim may represent a valid future strategy.

METHODS

Human samples

Peripheral blood samples were purified from buffy coats of healthy volunteer blood donors (independently of sex and age) under procedures approved by Institutional Review Board of Bambino Gesù Children' Hospital (Approval of Ethical Committee N° 1638/2019 prot. N° 19826), including informed consensus for research purpose. Blood cells were incubated with RosetteSep Human T cell enrichment cocktail antibody mix (StemCell 15061). Unlabeled Human Peripheral Blood T (hPBT) cells were isolated by density gradient over Lymphoprep (StemCell 07811), with centrifugation for 20min at 1200rcf. Then T cells have been collected, washed and used for subsequent analyses. Human colon adenocarcinoma tissue sections were collected from the archives of the Tumor Immunology Laboratory, Department of Health Science according to the Helsinki declaration and under the approval of the University of Palermo Ethical Review Board (Approval N° 09/2018).

Mice

WT and $Drp1^{fl/fl}$Lck:cre+ c57BL/6 mice were bred and maintained under conventional conditions at the Plaisant Srl (Castel Romano) Animal Facility. $Drp1^{fl/fl}$Lck:cre+ mouse strain has been previously described (15). Mice were kept in cages of no more than 5-6 mice each, divided by sex, under 12h/12h light/dark cycles, with standard temperature, humidity and pressure conditions according to FELASA guidelines. Small red squared mice house and paper were used for cage enrichment. Mice health was monitored daily by veterinary staff and health analysis for pathogens were performed every three months according to FELASA guidelines. All mice were sacrificed by neck dislocation at 2-3 months of age. All efforts were made to minimize animal suffering and to reduce the number of mice used, in accordance with the European Communities Council Directive of 24 November 1986 (86/609/EEC). The mice protocol has been approved by the Allevamenti Plaisant Srl Ethical Committee as well as by the Italian Ministry of Health (Authorization #186/2020-PR). It has been written following the ARRIVE Guidelines, and the numeric details have been chosen following the criteria described in The National Centre for the Replacement, Refinement and Reduction of Animals in Research (NC3Rs) (http://www.nc3rs.org.uk/). Sample size for the experiments performed has been established using power analysis method. Experiments involving growth of tumor cells in mice where performed using male mice.

Cell cultures and Reagents

Human Peripheral Blood T (hPBT) cells have been cultured in RPMI 1640 medium (Thermo Fisher 21875) supplemented with 10% Fetal Bovine Serum (Thermo Fisher 10270), 2mM L-glutamine (Thermo Fisher 25030081), 100U/ml penicillin/streptomycin (Thermo Fisher 15140130), 1x GIBCO MEM Non-essential amino-acids (Thermo Fisher 11140035), 1mM Sodium pyruvate (Thermo Fisher 11360039), and 100mg/ml Gentamycin (Thermo Fisher 15750045).

Murine T cells have been isolated from spleen using 70mm Cell Strainers (Corning 431751) and cultured in the same medium used for hPBT cells (complete RPMI medium) with the only exception of 50μM β-mercaptoethanol (Thermo Fisher 31350-010) addition.

MC38 tumor cells have been cultured in complete DMEM medium (Thermo Fisher 41966052) supplemented with 10% Fetal Bovine Serum (Thermo Fisher 10270), 2mM L-glutamine (Thermo Fisher 25030081), 100U/ml penicillin/streptomycin (Thermo Fisher 15140130), 1x GIBCO MEM Non-essential amino-acids (Thermo Fisher 11140035), 1mM Sodium pyruvate (Thermo Fisher 11360039), and 50μM β-mercaptoethanol (Thermo Fisher 31350-010).

Murine T cells have been isolated from spleen of WT mice and purified using Pan T Cell

Isolation Kit (Miltenyi 130-095-130) or naïve CD8+ T Cell Isolation Kit (Miltenyi 130-096-543).

For *in vitro* activation, $2x10^5$ murine T cells have been stimulated with 5mg/ml anti-CD3 (plate-coated) (eBioscience 14-0031-86) and 1mg/ml anti-CD28 (Invitrogen 14-0281-86) for up to 48h in 96well plate. Alternatively, $5x10^5$ murine or human T cells have been stimulated at 1:1 ratio in 48well plate in presence of Sulfate Latex 4% w/v 5um Beads (Molecular Probes S37227). For each experiment, $20x10^6$ beads were coated o.n. at 4°C with 2µg anti-CD3 (mouse: eBioscience 14-0031-86; human: eBioscience 16-0037-85) and 1µg anti-CD28 (mouse: Invitrogen 14-0281-86; human: 16-0289-85) and either 7µg of Recombinant PD-L1/B7-H1 Fc Chimera Protein (mouse: R&D System 1019-B7; human: R&D System 156-B7) (indicated as anti-CD3/28-PDL1-beads) or 7µg of Bovine Serum Albumin (Sigma A2153) (indicated as anti-CD3/28-beads). Cells defined as unstimulated were cultured in presence of beads coated with BSA only (o.n. coating of $20x10^6$ beads with 10µg of BSA). To modulate mTOR and ERK signaling, activated T cells have been incubated with 10nM RAD-001 (Novartis Oncology), 30µM FR180204 (Tocris 3706; indicated in the figures as ERKi) or 10 µM C6-Ceramide Cell-permeable ceramide analog (BML-SL110 Enzo Life Sciences). To inhibit autophagy, 20µM chloroquine (Sigma C6628) have been added to cells 1h before protein extraction.

To induce isolated murine naïve CD8+ T cells into an exhaustion-like state *in vitro*, cells have been stimulated up to 4 times with 5mg/ml anti-CD3 (plate-coated) (eBioscience 14-0031-86) and 1mg/ml anti-CD28 (Invitrogen 14-0281-86) for 24h in 96well plate. Between each stimulation, cells have been expanded using 20ng/ml mouse IL-2 (R&D System 402-ML). Cells were considered into exhaustion-like state after 4 stimulations (T_{ex}) and were compared with effector-like (T_{eff}) cells isolated from sibling mice and stimulated only once. For *in vitro* migration experiments, T_{ex} and T_{eff} cells were finally expanded *in vitro* for additional 6 days in IL2-containing medium and then used for the assays.

Western Blot

Western blot were performed as previously described (15). The following primary antibodies have been used: anti-actin (Cell Signaling 4970), anti-Drp1 (BD Bioscience 611113), anti-pS616-Drp1 (Cell Signaling 4494), anti-pS637-Drp1 (Cell Signaling 6319), anti-Mfn2 (Abcam ab56889), anti-Mfn1 (Santa Crux sc-50330), anti-Opa1 (BD Bioscience 612607), anti-Fis1 (Abcam ab71498), anti-Mff (Abcam ab129075), anti-pT202/204-ERK1/2 (Cell Signaling 4370), anti-ERK1/2 (Cell Signaling 4695), anti-Hsp90 (Cell Signaling 4877), anti-pSer2481-mTOR (Cell Signaling 2974), anti-mTOR (Cell Signaling 2983), anti-MnSOD (Enzo Life Sciences ADI-SOD-110), anti-LC3B (Cell Signaling 3868) and anti-GAPDH (Cell Signaling 2118). All primary antibody incubations were followed by incubation with appropriated secondary HRP-conjugated antibodies (GE Healthcare or Cell Signaling) in 5% milk plus 0.1% Tween20 (Sigma P2287). Detection of protein signals was performed using Clarity Western ECL substrate (Biorad 170-5061) and Amersham Imager 600. Stripping of the membranes for re-probing has been performed using buffer containing 1% Tween-20 (Sigma P2287), 0.1% SDS (Sigma 71729), and 0.2M glycine (VWR M103) at pH 2.2 (two washes for 10min). Original scan of western blot images shown throughout the manuscript are reported in Supplemental Figure 4.

Immunofluorescence

Immunofluorescence staining has been performed as previously described (16). Anti-TOM20 (Santa Cruz sc-11415) primary antibody was used to identify the mitochondrial network. Nunc Lab-Tek Chamber Slides (Thermo Fisher 154534) have been used to culture *in vitro* T cells directly on slides before fixation and were coated with 10ng/ml fibronectin (Millipore FC010) for 1h at RT before adding the cells. Images were acquired using a Perkin Elmer Ultraview VoX microscope. The mitochondrial network has been always evaluated upon 0.4mm slices z-stack reconstructions.

Immunohistochemistry

Formalin-fixed and paraffin embedded (FFPE) tissue samples of human colon cancer moderately differentiated (G2) cases were selected for *in situ* immunophenotypical analyses. Four-micrometers-thick sections were deparaffinized, rehydrated and unmasked using Novocastra Epitope Retrieval Solutions pH 9 in PT Link Dako at 98°C for 30 minutes. Subsequently, the sections were brought to room temperature and washed in PBS. After neutralization of the endogenous peroxidase with 3% H_2O_2 and Fc blocking by a specific protein block (Novocastra), the samples were incubated with anti-pSer616-Drp1 (clone D9A1 Cell Signaling, 1:100) and anti-PD-1 (clone NAT105 Abcam, 1:50) antibodies. IHC staining was revealed using "MACH 2 Double Stain 1" kit and DAB (3,3'- Diaminobenzidine, Novocastra) and Vulcan Fast Red or Ferangi Blue as substrate-chromogens. Slides were analyzed under a Zeiss Axioscope A1 and microphotographs were collected using a Zeiss Axiocam 503 Color with the Zen 2.0 Software (Zeiss).

Flow Cytometry

The following antibodies have been used to stain extracellular proteins: anti-CD8-Alexa488 (Biolegend 100723), anti-PD1-PE (eBioscience 12-9981-83), anti-CD4-PECy7 (Biolegend 100422), antiCD45-BV650 (Biolegend 103151), anti-CD44-BV421 (Biolegend 103039). Foxp3 Transcription Factor Staining Buffer Set (00-5523-00, eBioscience) has been used to stain intracellular proteins, detected with the following antibodies: anti-Drp1 (BD Bioscience 611113), anti-pS616-Drp1 (Cell Signaling 4494), anti-pS637-Drp1 (Cell Signaling 6319), anti-Mfn2 (Abcam ab56889), anti-Mfn1 (Santa Crux sc-50330), anti-Opa1 (BD Bioscience 612607), anti-Fis1 (Abcam ab71498), anti-Mff (Abcam ab129075), secondary goat anti-rabbit Alexa647 (Invitrogen A21244), secondary goat anti-mouse Alexa647 (Jackson 115-605-146), secondary goat anti-rabbit Alexa405 (Invitrogen A31556). Primary antibodies were incubated o.n. at 4°C, while secondary antibodies for 1h at RT. Background signals obtained by staining solely with secondary antibodies were subtracted from the corresponding signal from primary antibodies in the same cells to obtain MFI values reported in the figures.

To evaluate IFNγ production in tumor-derived T cells, cells have been restimulated for 4h in presence of 50ng/ml PMA (Sigma 79346), 1µg/ml ionomycin (Sigma I9657) and 2µM monensin (added for the last 2h, Sigma M5273) and then fixed and processed using Foxp3 Transcription Factor Staining Buffer Set (00-5523-00, eBioscience) and anti-IFNg antibody (eBioscience 12-7311-82). Acquisitions have been performed using BD Accuri C6 and BD FACSCelesta cytometers. Cell sorting have been performed by staining cells with the aforementioned extracellular antibodies and using BD FACS Aria III flow cytometer.

For the evaluation of the mitochondrial membrane potential, 1mM TMRE (Thermo Fisher T669) has been added for 20 min and then the cells were washed and analysed. As a positive control for mitochondria depolarization, cells have been pre-treated with 50µM FCCP (Sigma Aldrich C2920).

Tumor induction

$5*10^5$ MCA38 cells were injected subcutaneously into the right flank of two months-old male WT or $Drp1^{fl/fl}$ and $Drp1^{fl/fl}$Lck:cre+ mice. Mice were kept for up to 17/18 days in animal facility, and tumor growth was monitored twice or three times per week and recorded as [longest diameter]*[shortest diameter]^2 in cubic millimetres. At days 7, 9, 11, 14 and 16 from tumor inoculation, mice were inoculated i.p. with 150µg of InVivoMab anti-mouse PD-1 (CD279), clone RMP1-14 (Bioxcell, BE0146) or 150µg InVivoMab rat IgG2a isotype control, clone 2A3 (Bioxcell, BE0089) antibodies (in 150µl of saline). Mice were randomly subdivided into each experimental group (a-IgG or a-PD1) before inoculation of antibodies (no specific randomization method was used). At day 17, mice were sacrificed and tumors were collected. Tumor tissues were mechanically

dissociated over 70 mm-cell strainers, and mononuclear cells were enriched from tumor-derived cell suspensions by 40%/80% Percoll (GE Healthcare GE17-0891-01) density gradient, by collecting cells at the interface between 40% and 80% Percoll solution.

Isolated TILs have been used for subsequent proliferation and migration *in vitro* analyses or stained for flow cytometric measurements.

Seahorse analysis

Basal OCR has been measured in T cells during acute phase (unstimulated or stimulated for 12h) or after 48h of stimulation and 4 days of *in vitro* expansion with IL2, as previously described (15).

***In vitro* proliferation and migration assays**

To evaluate the *in vitro* proliferation potential of tumor-infiltrated CD8+ T cells isolated from tumor-bearing $Drp1^{fl/fl}$ and $Drp1^{fl/fl}$Lck:cre+ mice, $2x10^5$ isolated TILs have been cultured *in vitro* in 96well plate in presence of 20ng/ml mouse IL-2 (R&D System 402-ML), 20ng/ml mouse IL-7 (R&D System 407-ML) and 20ng/ml mouse IL-15 (R&D System 447-ML). The total number of cells were estimated each 2/3 days using BD Accuri C6 flow cytometer and the percentage of CD8+ T cells in each plate evaluated by flow cytometry staining with anti-CD8-A488 (Biolegend 100723) antibody.

For transwell migration assays, $5x10^5$ TILs or *in vitro*-induced T_{eff} and T_{ex} have been starved from serum for 2h (by replacing FBS in the medium with 0.5% Bovine Serum Albumine, Sigma A2153) and then loaded on 5mm-pore size transwell filters (Costar 3421) and allowed to migrate for 2h in presence of 25nM CCL19 (R&D System 440-M3), 50nM CCL21 (R&D System 457-6C) or 10% Fetal Bovine Serum (Thermo Fisher 10270).

For the polarization assay, $2x10^5$ cells have been starved from serum for 2h (by replacing FBS in the medium with 0.5% Bovine Serum Albumine, Sigma A2153). Then, cells were allowed to adhere to 10mg/ml fibronectin-coated (Millipore FC010) microscope slides (Thermo Fisher ER302W-CE24) for 30min and stimulated by adding 50nM CCL19 (R&D System 440-M3) and 50nM CCL21 (R&D System 457-6C) for 15min before fixation and immunostaining. Alternatively, after serum starvation, $2x10^6$ cells were kept in 1.5ml Eppendorf tube and stimulated by adding 50nM CCL19 (R&D System 440-M3) and 50nM CCL21 (R&D System 457-6C) for 15min before directly proceeding to protein extraction.

Statistical Analysis

In the Figure legends, "n" indicates either the number of independent experiments (*in vitro* primary cells) or the number of mice used. Data are expressed as mean ± SEM from at least three independent experiments unless specified otherwise (Microsoft Office Excel and SigmaPlot v12.5 have been used for analysis). The number of mice used has been estimated using the power analysis method. All the acquisitions of the experiments have been performed blinded without knowing the specific conditions of each sample. Comparisons between groups were done using two-tailed Student's T-test (two groups) or One-way and Two-way ANOVA (multiple groups and repeated measurements, adjustments for pairwise comparisons were performed using Holm-Sidak method). Mann-Whitney Rank Sum Test or ANOVA on ranks have been used if samples did not meet assumptions of normality and/or equal variance. Chi-square test has been used to evaluate data in Figure 1B. P-values are indicated in the Figures as follows: * = $p < 0.05$, ** = $p < 0.01$, *** = $p < 0.001$.

AUTHOR CONTRIBUTIONS

LS and SC conceived the research and wrote the manuscript. LS performed most of the experiments. YA helped performing western blots and isolation of cells from tumors. VC and CT performed immunohistochemistry analyses on human tumor samples. AC, CP and GM performed seahorse analysis. SC raised funding. All authors approved the manuscript.

ACKNOWLEDGMENTS

This work was funded by Fondazione AIRC (Grant IG-2017 19826) to SC. LS was supported by a Fondazione AIRC “Fellowship for Italy” (23926).

CONFLICT OF INTEREST

The authors declare no conflict of interest.

REFERENCES

1. Sharpe AH, Pauken KE. The diverse functions of the PD1 inhibitory pathway. *Nat. Rev. Immunol.* 2018;18(3):153–167.

2. Okazaki T, Honjo T. PD-1 and PD-1 ligands: from discovery to clinical application. *Int. Immunol.* 2007;19(7):813–824.

3. Parry R V. et al. CTLA-4 and PD-1 receptors inhibit T-cell activation by distinct mechanisms. *Mol. Cell. Biol.* 2005;25(21):9543–9553.

4. Patsoukis N et al. Selective Effects of PD-1 on Akt and Ras Pathways Regulate Molecular Components of the Cell Cycle and Inhibit T Cell Proliferation. *Sci. Signal.* 2012;5(230):ra46–ra46.

5. Jubel JM, Barbati ZR, Burger C, Wirtz DC, Schildberg FA. The Role of PD-1 in Acute and Chronic Infection. *Front. Immunol.* 2020;11:487.

6. Wherry EJ, Kurachi M. Molecular and cellular insights into T cell exhaustion. *Nat Rev Immunol* 2015;15(8):486–499.

7. Sun C, Mezzadra R, Schumacher TN. Regulation and Function of the PD-L1 Checkpoint. *Immunity* 2018;48(3):434–452.

8. Iwai Y, Hamanishi J, Chamoto K, Honjo T. Cancer immunotherapies targeting the PD-1 signaling pathway. *J. Biomed. Sci.* 2017;24(1):26.

9. Zamani MR, Aslani S, Salmaninejad A, Javan MR, Rezaei N. PD-1/PD-L and autoimmunity: A growing relationship. *Cell. Immunol.* 2016;310:27–41.

10. Simula L, Nazio F, Campello S. The Mitochondrial dynamics in cancer and immune-surveillance. *Semin. Cancer Biol.* 2017;47:29–42.

11. Alavi M V, Fuhrmann N. Dominant optic atrophy, OPA1, and mitochondrial quality control: understanding mitochondrial network dynamics. *Mol Neurodegener* 2013;8:32.

12. Eura Y, Ishihara N, Yokota S, Mihara K. Two mitofusin proteins, mammalian homologues of FZO, with distinct functions are both required for mitochondrial fusion. *J Biochem* 2003;134(3):333–344.

13. Otera H, Ishihara N, Mihara K. New insights into the function and regulation of mitochondrial fission. *Biochim Biophys Acta* 2013;1833(5):1256–1268.

14. Losón OC, Song Z, Chen H, Chan DC. Fis1, Mff, MiD49, and MiD51 mediate Drp1 recruitment in mitochondrial fission. *Mol Biol Cell* 2013;24(5):659–667.

15. Simula L et al. Drp1 Controls Effective T Cell Immune-Surveillance by Regulating T Cell Migration, Proliferation, and cMyc-Dependent Metabolic Reprogramming. *Cell Rep.* 2018;25(11):3059–3073.

16. Simula L et al. JNK1 and ERK1/2 modulate lymphocyte homeostasis via BIM and DRP1 upon AICD induction. *Cell Death Differ.* 2020;1–19.

17. Baixauli F et al. The mitochondrial fission factor dynamin-related protein 1 modulates T-cell receptor signalling at the immune synapse. *EMBO J* 2011;30(7):1238–1250.

18. Wang R et al. The transcription factor Myc controls metabolic reprogramming upon T lymphocyte activation. *Immunity* 2011;35(6):871–882.

19. Ma EH et al. Metabolic Profiling Using Stable Isotope Tracing Reveals Distinct Patterns of Glucose Utilization by Physiologically Activated CD8+ T Cells. *Immunity* 2019;51(5):856-870.e5.

20. Munford H, Dimeloe S. Intrinsic and Extrinsic Determinants of T Cell Metabolism in Health and Disease. *Front. Mol. Biosci.* 2019;6. doi:10.3389/fmolb.2019.00118

21. Zinselmeyer BH et al. PD-1 promotes immune exhaustion by inducing antiviral T cell motility paralysis. *J Exp Med* 2013;210(4):757–774.

22. Patsoukis N et al. PD-1 alters T-cell metabolic reprogramming by inhibiting glycolysis and promoting lipolysis and fatty acid oxidation. *Nat. Commun.* 2015;6(1):6692.

23. Buck MD et al. Mitochondrial Dynamics Controls T Cell Fate through Metabolic Programming. *Cell* 2016;166(1):63–76.

24. Dunsford LS, Thoirs RH, Rathbone E, Patakas A. A Human In Vitro T Cell Exhaustion Model for Assessing Immuno-Oncology Therapies. In: *Methods in Pharmacology and Toxicology*. 2020:89–101

25. Kashatus JA et al. Erk2 phosphorylation of Drp1 promotes mitochondrial fission and MAPK-driven tumor growth. *Mol Cell* 2015;57(3):537–551.

26. Simula L, Campanella M, Campello S. Targeting Drp1 and mitochondrial fission for therapeutic immune modulation. *Pharmacol. Res.* 2019;146:104317.

27. Morita M et al. mTOR Controls Mitochondrial Dynamics and Cell Survival via MTFP1. *Mol Cell* 2017;67(6):922-935.e5.

28. Darvishi B, Farahmand L, Eslami-S Z, Majidzadeh-A K. NF-κB as the main node of resistance to receptor tyrosine kinase inhibitors in triple-negative breast cancer. *Tumor Biol.* 2017;39(6):101042831770691.

29. Mendoza MC, Er EE, Blenis J. The Ras-ERK and PI3K-mTOR pathways: cross-talk and compensation. *Trends Biochem Sci* 2011;36(6):320–328.

30. Sedrani R, Cottens S, Kallen J, Schuler W. Chemical modification of rapamycin: the discovery of SDZ RAD. *Transplant. Proc.* 1998;30(5):2192–2194.

31. Ohori M et al. Identification of a selective ERK inhibitor and structural determination of the inhibitor–ERK2 complex. *Biochem. Biophys. Res. Commun.* 2005;336(1):357–363.

32. Raines MA, Kolesnick RN, Golde DW. Sphingomyelinase and ceramide activate mitogen-activated protein kinase in myeloid HL-60 cells. *J. Biol. Chem.* 1993;268(20):14572–14575.

33. Grasselly C et al. The Antitumor Activity of Combinations of Cytotoxic Chemotherapy and Immune Checkpoint Inhibitors Is Model-Dependent. *Front. Immunol.* 2018;9(OCT). doi:10.3389/fimmu.2018.02100

34. Campello S et al. Orchestration of lymphocyte chemotaxis by mitochondrial dynamics. *J Exp Med* 2006;203(13):2879–2886.

35. Siska PJ et al. Mitochondrial dysregulation and glycolytic insufficiency functionally impair CD8 T cells infiltrating human renal cell carcinoma. *JCI Insight* 2017;2(12). doi:10.1172/jci.insight.93411

36. Qian W et al. Mitochondrial hyperfusion induced by loss of the fission protein Drp1 causes ATM-dependent G2/M arrest and aneuploidy through DNA replication stress. *J Cell Sci* 2012;125(Pt 23):5745–5757.

37. Caruana I, Simula L, Locatelli F, Campello S. T lymphocytes against solid malignancies: winning ways to defeat tumours. *Cell Stress* 2018;2(8):200–212.

38. Chen J et al. NR4A transcription factors limit CAR T cell function in solid tumours. *Nature* 2019;567(7749):530–534.

39. Pauken KE, Wherry EJ. Overcoming T cell exhaustion in infection and cancer. *Trends Immunol.* 2015; doi:10.1016/j.it.2015.02.008

40. Mandal CC, Mehta J, Prajapati VK. Programmed Death 1 (PD1)-Mediated T-Cell Apoptosis and Cancer Immunotherapy. In: *Apoptosis and Beyond*. Hoboken, NJ, USA: John Wiley & Sons, Inc.; 2018:695–722

41. Ogando J et al. PD-1 signaling affects cristae morphology and leads to mitochondrial dysfunction in human CD8+ T lymphocytes. *J. Immunother. Cancer* 2019;7(1):151.

42. Cogliati S, Enriquez JA, Scorrano L. Mitochondrial Cristae: Where Beauty Meets Functionality. *Trends Biochem. Sci.* 2016; doi:10.1016/j.tibs.2016.01.001

43. Sarin M et al. Alterations in c-Myc phenotypes resulting from dynamin-related protein 1 (Drp1)-mediated mitochondrial fission. *Cell Death Dis.* 2013;4(6):e670–e670.

44. Buck MD, O'Sullivan D, Pearce EL. T cell metabolism drives immunity. *J Exp Med* 2015;212(9):1345–1360.

45. Twig G et al. Fission and selective fusion govern mitochondrial segregation and elimination by autophagy. *EMBO J* 2008;27(2):433–446.

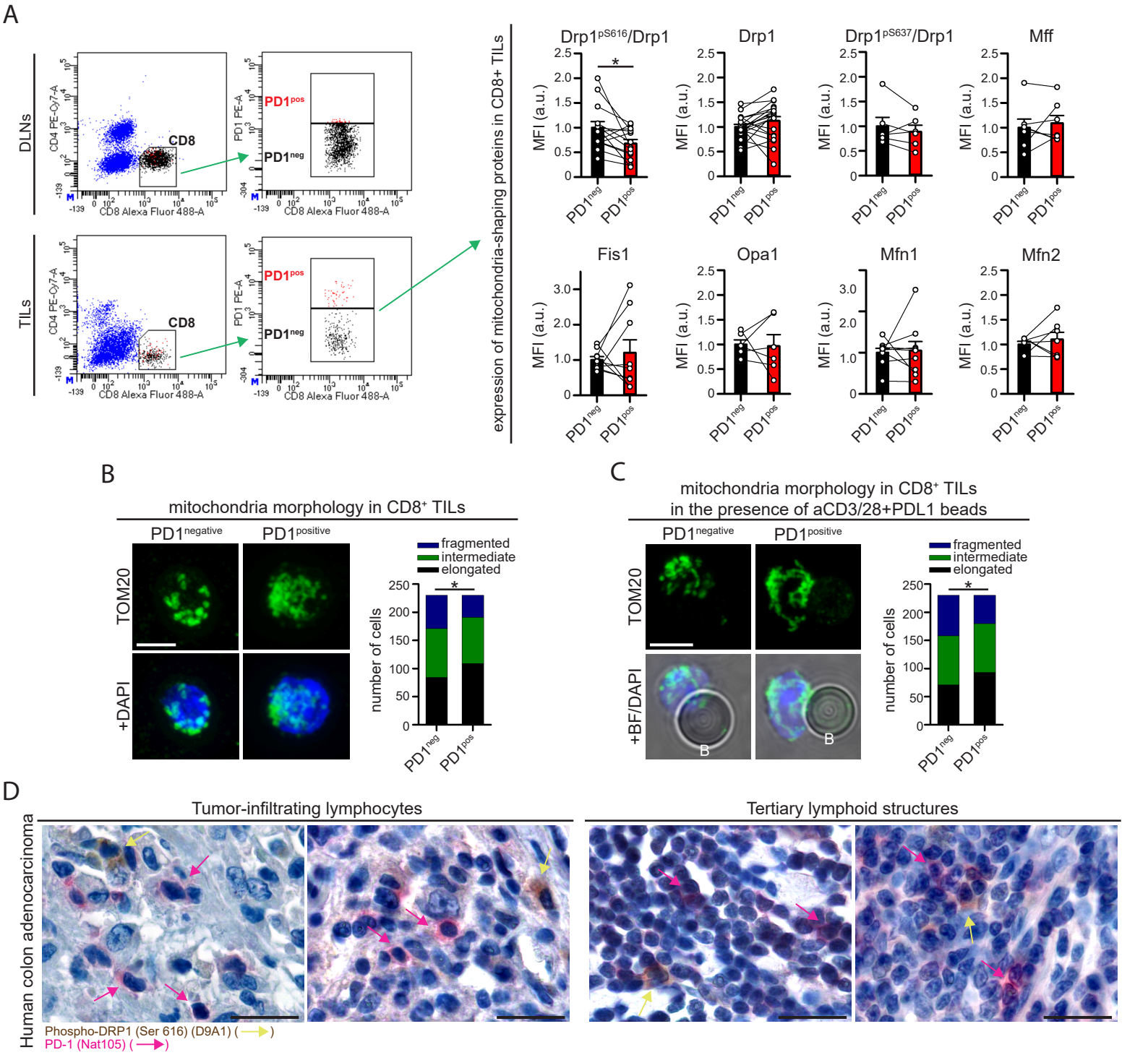

Figure 1. PD1positive and PD1negative CD8+ T cells within MC38-derived tumor microenvironment show different mitochondria morphologies.

(**A**) Tumor-infiltrating lymphocytes have been isolated from 18 days-old MC38-derived tumor mass grown in WT c57BL/6 mice and the expression of the indicated mitochondria-shaping proteins have been evaluated into PD1^{negative} (PD1^{neg}) and PD1^{positive} (PD1^{pos}) CD8+ T cell subpopulations. Representative gating strategy to distinguish PD1^{neg} and PD1^{pos} CD8+ T cells is shown on the left. Graphs on the right indicate the normalized median fluorescence intensity (MFI) of the indicated proteins evaluated by intracellular flow cytometry in PD1^{neg} and PD1^{pos} CD8+ T cells from the same mice (pS616-Drp1 n=14; Drp1 n=20; Mfn1 and Fis1 n=9; Mfn2 and Mff n=7; Opa1 and pS637-Drp1 n=6; paired t-tests). (**B-C**) PD1^{negative} (PD1^{neg}) and PD1^{positive} (PD1^{pos}) CD44+ CD45+ CD8+ T cells have been sorted and purified form 18 days-old MC38-derived tumor mass grown in WT c57BL/6 mice. Gating strategy is shown in Supplemental Figure 1. Mitochondria morphology was evaluated by immunofluorescence (anti-TOM20 staining) and upon z-stack reconstruction. In (B) cells have been fixed immediately after purification and processed for immunostaining. In (C) cells have been stimulated for 2h in the presence of beads coated with aCD3/28 Abs plus PDL1 and then fixed and processed for immunostaining. For each panel, representative images of the observed mitochondria morphologies are shown on the left, while graphs on the right show the distribution of cells into the indicated category according to mitochondria morphology in PD1^{neg} and PD1^{pos} CD8+ T cells (n=230 cells each condition from 8 (unstimulated) or 10 (stimulated with beads) pooled mice; chi-square tests). (**D**) Representative microphotographs of double-marker immunohistochemistry for PD1 (rose; rose arrows) and Drp1-pSer616 (brown; yellow arrows) expression in lymphoid elements infiltrating human colon cancer.

Data are shown as mean ± SEM. Scale bar: 5μm in **B** and **C** and 50μm in **D**. Significance is indicated as follows: *=p<0.05.

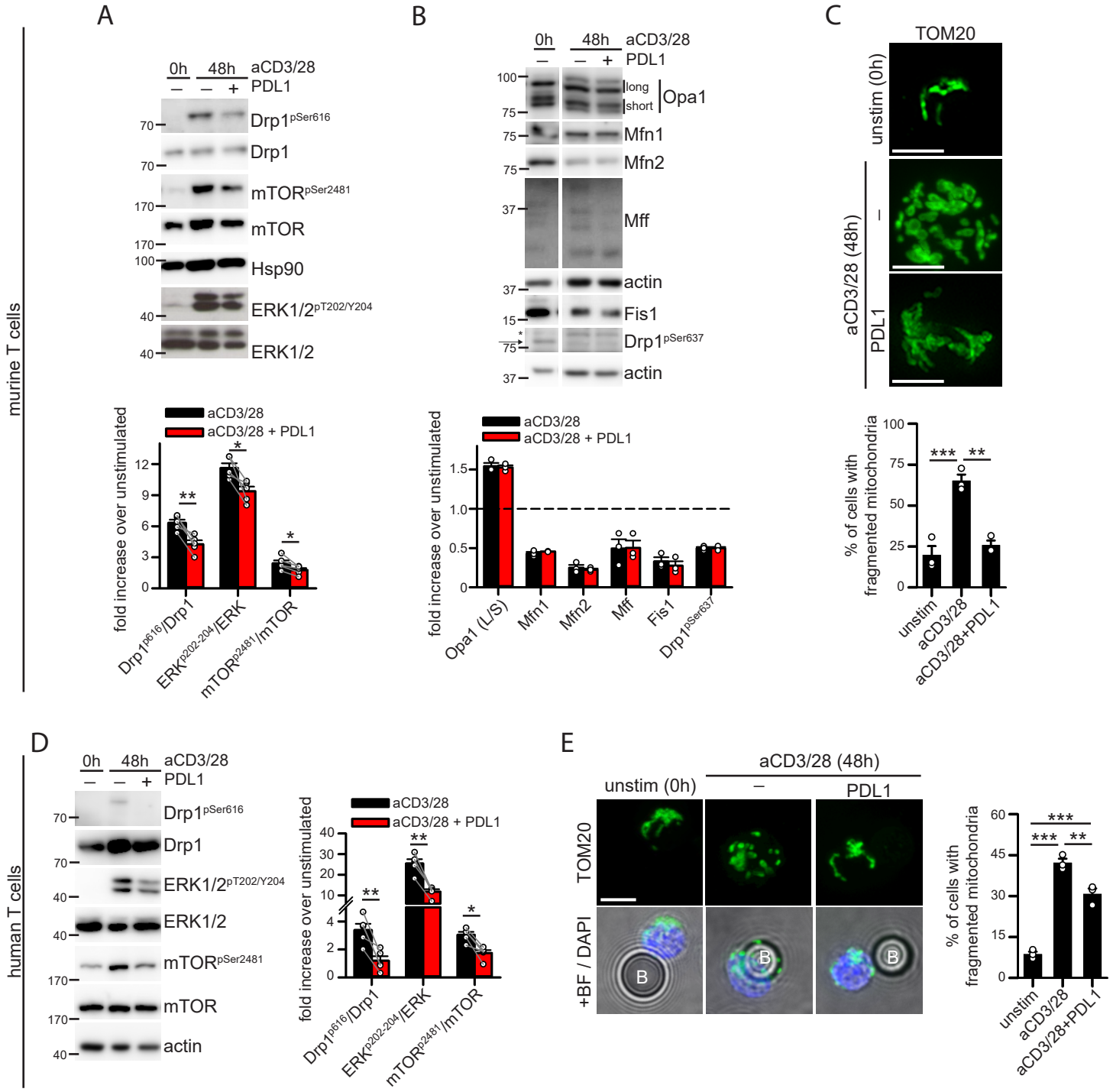

Figure 2. PD1 signaling downregulates Drp1-dependent mitochondria fragmentation in murine and human T cells.
(**A-B**) Murine T cells have been isolated from spleen of WT c57BL/6 mice and left unstimulated (0h) or stimulated for 48h with anti-CD3/28- or anti-CD3/28-PDL1-beads. The expression level of the indicated (phospho)-proteins has been evaluated by western blot (A n=5, paired t-tests; B n=3). (**C**) Representative immunofluorescence images showing the mitochondrial network (anti-TOM20 staining) in murine T cells isolated and stimulated as in (A). Quantification of the percentage of cells showing fragmented mitochondria in each condition is reported in the graph below (n=3). (**D**) Human T cells have been isolated from peripheral blood and left unstimulated (0h) or stimulated for 48h with anti-CD3/28- or anti-CD3/28-PDL1-beads. The expression level of the indicated (phospho)-proteins has been evaluated by western blot (n=5; paired t-tests). (**E**) Representative immunofluorescence images showing the mitochondrial network (anti-TOM20 staining; "B" indicates a bead) in human T cells isolated and stimulated as in (C). Quantification of the percentage of cells showing fragmented mitochondria in each condition is reported in the graph on the right (n=3).
Data are shown as mean ± SEM. Scale bar: 5µm in **C** and **E**. Significance is indicated as follows: *=p<0.05; **=p<0.01; ***=p<0.001.

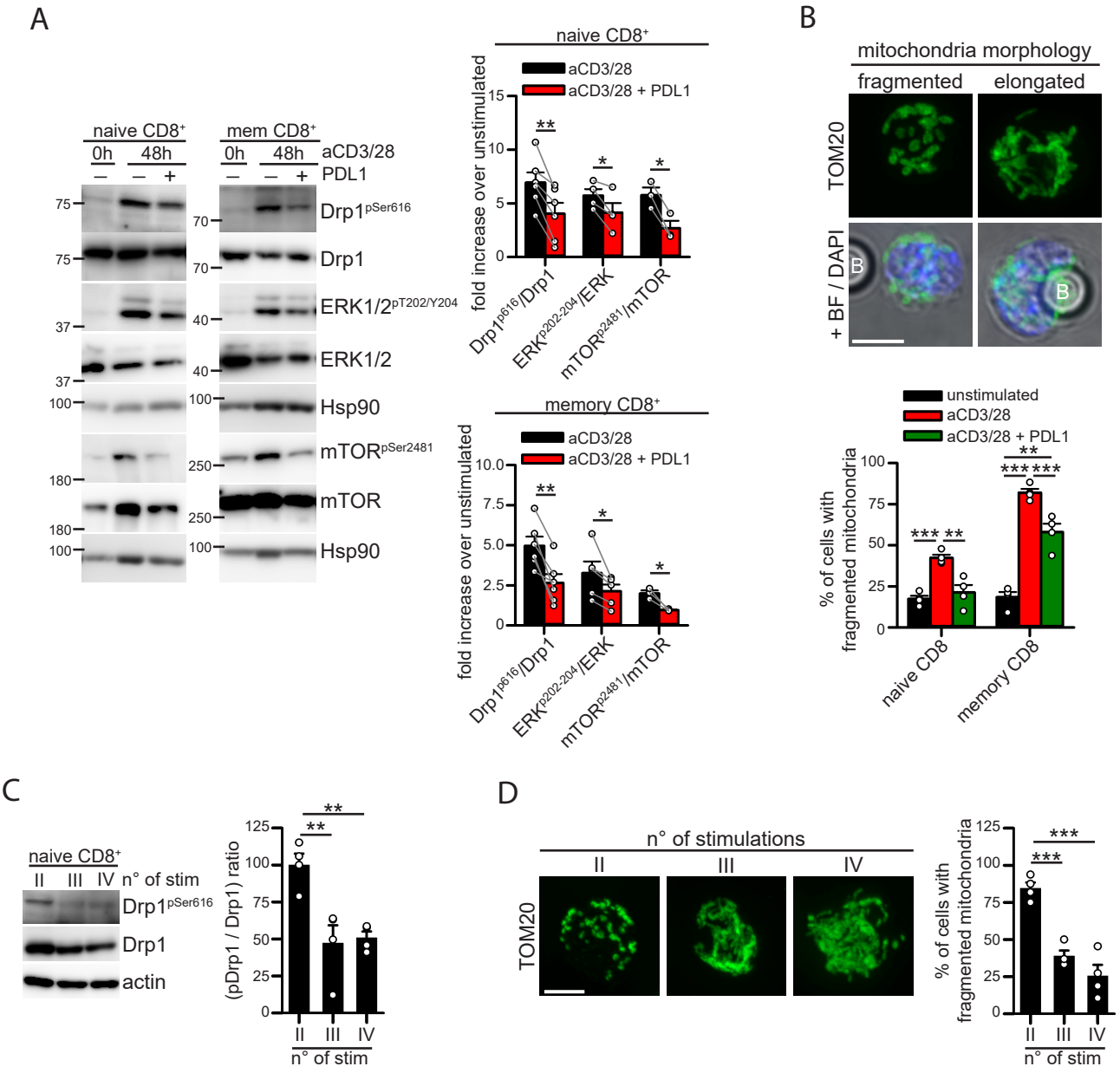

Figure 3. PD1 signaling downregulates Drp1-dependent mitochondria fragmentation in both naïve and memory murine CD8+ T cells, as it is observed upon repeated cycle of in vitro stimulation in naïve CD8+ T cells.

(**A**) Murine CD44^{neg} naïve and CD44^{pos} memory (mem) CD8+ T cells have been isolated from spleen of WT c57BL/6 mice and left unstimulated (0h) or stimulated for 48h with anti-CD3/28- or anti-CD3/28-PDL1-beads. The expression level of the indicated (phospho)-proteins has been evaluated by western blot in both naïve and memory CD8+ T cells (pDrp1 n=6; pERK naive n=4; pERK memory n=5; p-mTOR n=3; paired t-tests). (**B**) Immunofluorescence images showing representative mitochondrial morphologies (anti-TOM20 staining; "B" indicates a bead) observed in CD44^{neg} naïve and CD44^{pos} memory CD8+ T cells isolated and stimulated as in (A). Quantification of the percentage of cells showing fragmented mitochondria in each condition is reported in the graph below (n=4). (**C**) Murine CD44^{neg} naïve CD8+ T cells have been isolated from spleen of WT c57BL/6 mice and stimulated up to 4 times with plate-coated anti-CD3 Ab plus soluble anti-CD28 for 24h. After each stimulation, cells were left to recover 6 days in IL2-containing medium before the next stimulation. The expression level of the indicated (phospho)-proteins has been evaluated by western blot immediately after the second (II), third (III) and fourth (IV) stimulation (n=4). (**D**) Representative immunofluorescence images showing the mitochondrial network (anti-TOM20 staining) in murine CD44^{neg} naïve CD8+ T cells stimulated as in (C). Quantification of the percentage of cells showing fragmented mitochondria in each condition is reported in the graph on the right (n=4).

Data are shown as mean ± SEM. Scale bar: 5µm in **B** and **D**. Significance is indicated as follows: *=p<0.05; **=p<0.01; ***=p<0.001.

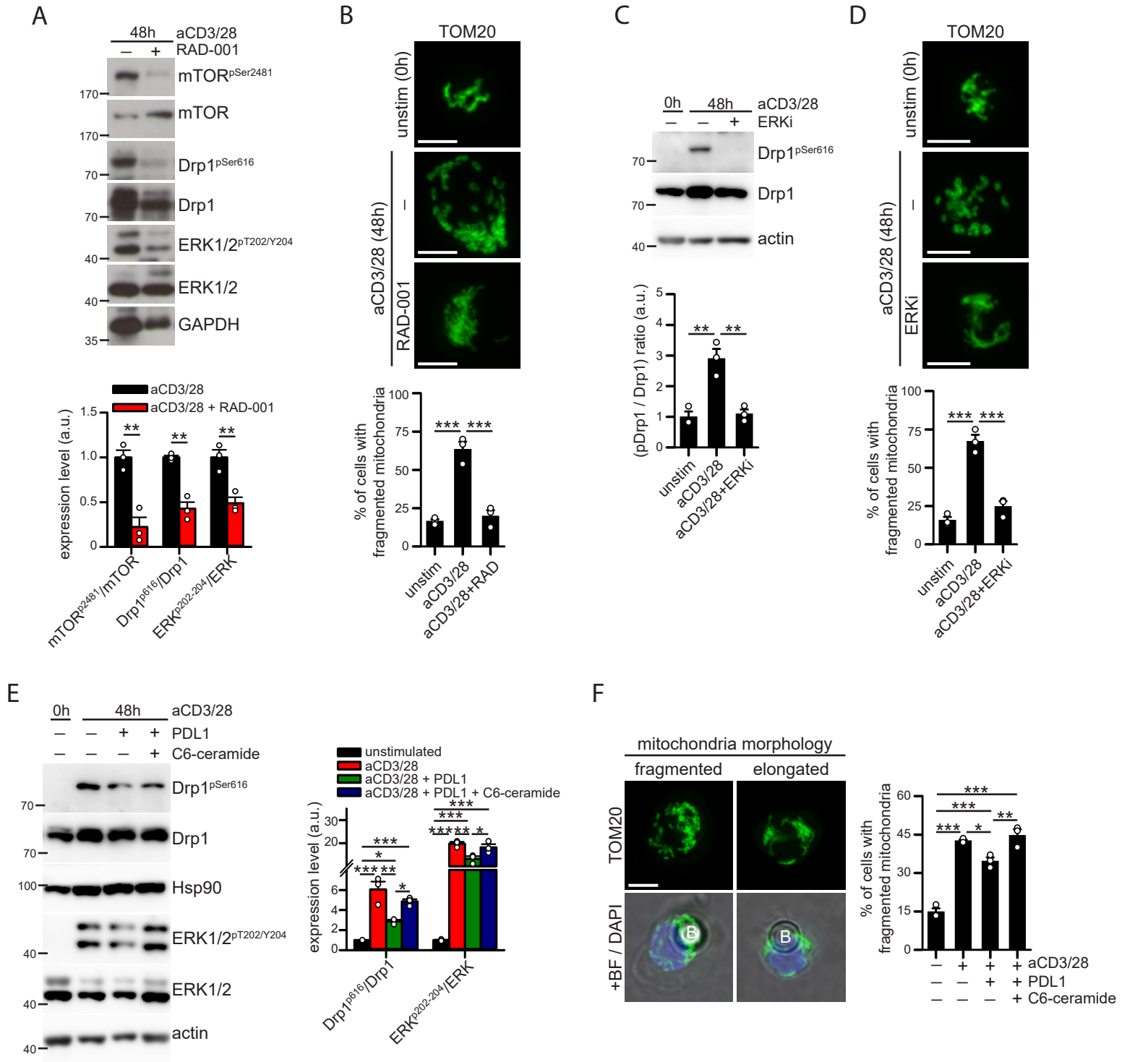

Figure 4. PD1 signaling down-modulates Drp1 activity via ERK and mTOR pathways.

(**A-D**) Murine T cells have been isolated from spleen of WT c57BL/6 mice and stimulated for 48h with anti-CD3/28-coated beads in presence or not of 10nM RAD-001 (mTOR inhibitor; A-B) or 30μM FR180204 (ERK inhibitor: ERKi; C-D). In (A) and (C) is reported the expression level of the indicated (phospho)-proteins evaluated by western blot and quantified in the graphs below (n=3). In (B) and (D) are reported representative immunofluorescence images showing the mitochondrial network (anti-TOM20 staining) in murine T cells isolated. Quantification of the percentage of cells showing fragmented mitochondria in each condition is reported in the graphs below (n=3). (**E**) hPBT cells have been isolated from spleen of WT c57BL/6 mice and stimulated for 48h with anti-CD3/28- or anti-CD3/28-PDL1-beads in presence or not of 10μM C6-ceramide. The expression level of the indicated (phospho)-proteins has been evaluated by western blot and quantified in the graph on the right (n=3). (**F**) Immunofluorescence images showing representative mitochondrial morphology (anti-TOM20 staining; "B" indicates a bead) observed in hPBT cells isolated and stimulated as in (E). Quantification of the percentage of cells showing fragmented mitochondria in each condition is reported in the graph on the right (n=3).

Data are shown as mean ± SEM. Scale bar: 5μm in **B**, **D** and **F**. Significance is indicated as follows: *=p<0.05; **=p<0.01; ***=p<0.001.

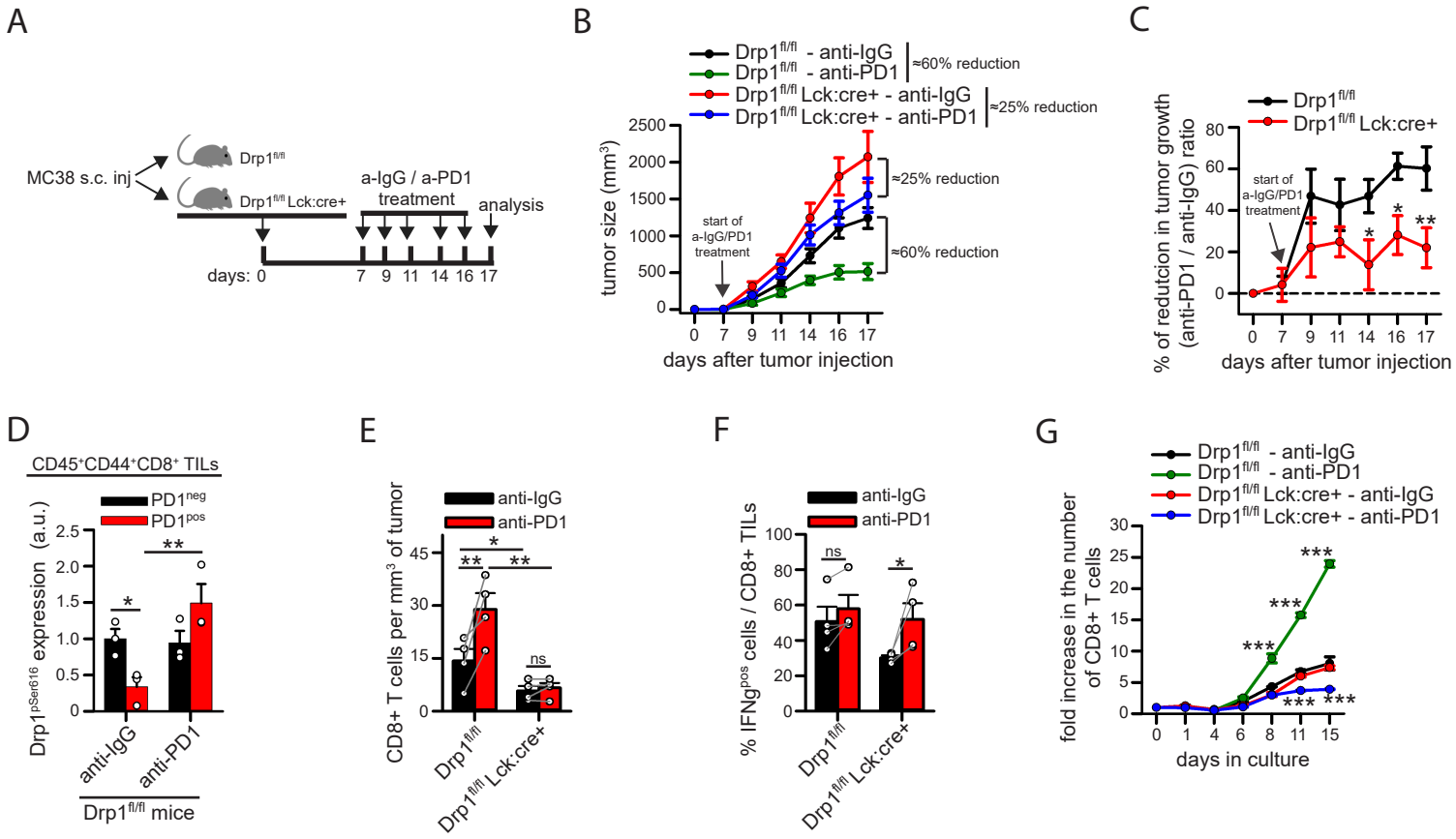

Figure 5. The downregulation of Drp1 activity in tumor-derived PD1positive T cells contributes to tumor growth.
(**A**) Schematic representation of the experimental plan. (**B**) Size of MC38-derived tumors grown for the indicated days in control Drp1$^{fl/fl}$ or conditional-KO Drp1$^{fl/fl}$Lck:cre+ mice inoculated with anti-IgG or anti-PD1 antibodies as indicated in (A) (Drp1$^{fl/fl}$ anti-IgG n=8; Drp1$^{fl/fl}$ anti-PD1 and Drp1$^{fl/fl}$Lck:cre+ anti-IgG n=12; Drp1$^{fl/fl}$Lck:cre+ anti-PD1 n=14). (**C**) Relative percentage of the reduction in tumor growth (anti-PD1 / anti-IgG ratio) calculated from data in (B) for control Drp1$^{fl/fl}$ or conditional-KO Drp1$^{fl/fl}$Lck:cre+ mice (Drp1$^{fl/fl}$ n=12; Drp1$^{fl/fl}$Lck:cre+ n=14). (**D**) Quantification of the Drp1-pSer616 median fluorescence intensity (MFI) evaluated by intracellular flow cytometry in CD45+ CD44+ CD8+ PD1^{neg} and PD1^{pos} TILs from control Drp1$^{fl/fl}$ mice. The MFI value obtained in corresponding TILs from conditional-KO Drp1f$^{fl/fl}$Lck:cre+ mice has been used as negative control and subtracted from the corresponding population in Drp1$^{fl/fl}$ mice to obtain pSer616-Drp1 MFI data reported in the graph (n=3). (**E**) Absolute number of CD8+ T cells per mm^3 of tumor collected from MC38-derived tumor masses grown for 17 days as described in (A) (n=4; Two-Way ANOVA on repeated measurements). (**F**) TILs have been isolated from MC38-derived tumor masses grown for 17 days as described in (A) and stimulated *in vitro* for 4h to evaluate IFNγ production. Percentage of IFNγ^{pos} cells among CD8+ T cells in each condition is reported in the graph (n=4; Two-Way ANOVA on repeated measurements). (**G**) TILs have been isolated from MC38-derived tumor masses grown for 17 days as described in (A) and cultured in vitro for the indicated days in presence of IL-2, IL-7 and IL-15 cytokines. Quantification of the fold increase in the absolute number of CD8+ T cells per day (starting value at day 0 = 1) is reported in the graph. Significance is indicated for each single point only if that day the population differs statistically from all the other 3 populations (n=3).
Data are shown as mean ± SEM. Significance is indicated as follows: *=p<0.05; **=p<0.01; ***=p<0.001.

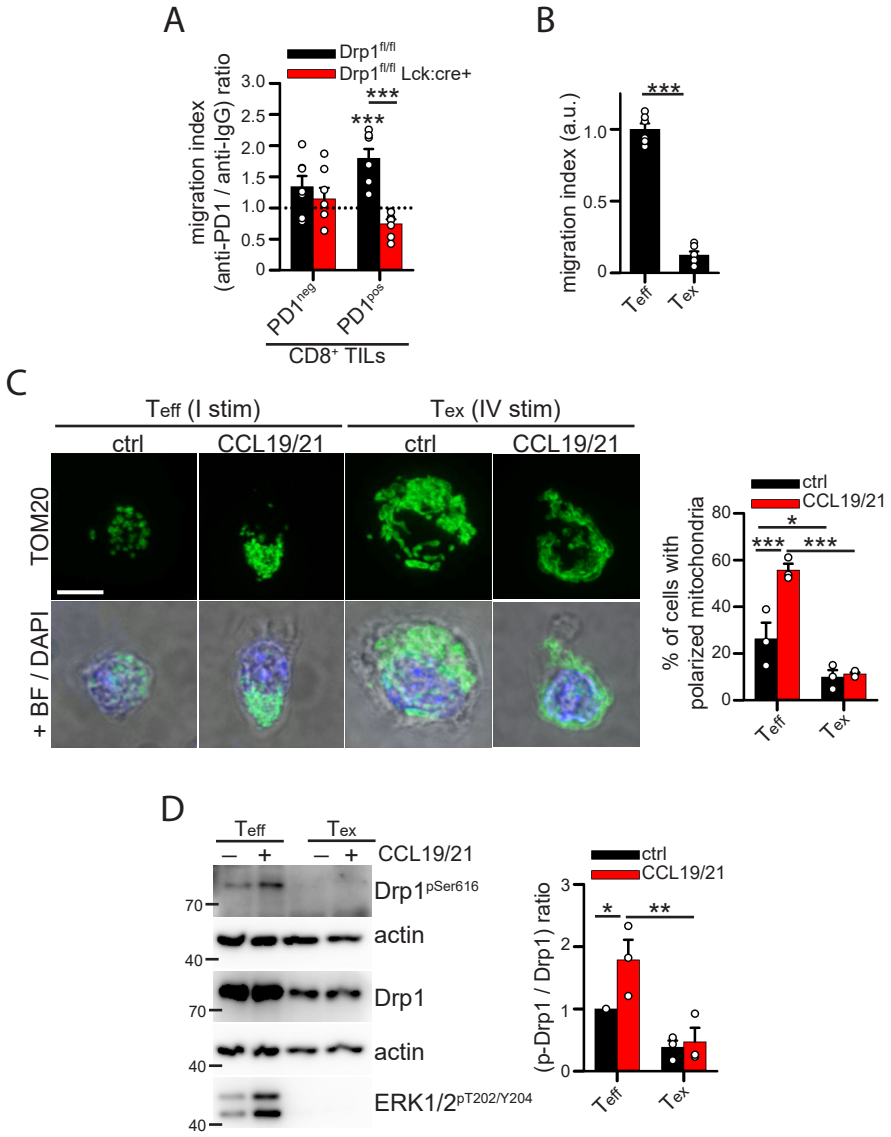

Figure 6. The downregulation of Drp1 activity contributes to the reduced motility of PD1positive T cells.
(**A**) TILs have been isolated from MC38-derived tumor masses grown for 17 days in control Drp1$^{fl/fl}$ or conditional-KO Drp1$^{fl/fl}$Lck:cre+ mice inoculated with anti-IgG or anti-PD1 antibodies as indicated in Fig. 5A. Then, TILs were starved from serum for 2h and allowed to migrate in response to 10% Fetal Bovine Serum for 2h using transwell migration assay. The graph indicates the relative (anti-PD1 / anti-IgG) migration index calculated for PD1^{neg} and PD1^{pos} CD8+ TILs isolated from tumor-bearing control Drp1$^{fl/fl}$ or conditional-KO Drp1$^{fl/fl}$Lck:cre+ mice inoculated with anti-IgG or anti-PD1 antibodies as indicated in Fig. 5A (n=7). (**B**-**D**) Murine exhausted T cells (Tex) have been generated in vitro through 4 cycles of a-CD3/28-mediated stimulation (24h) and IL2-mediated expansion (6 days) and compared to effector T cells (Teff) generated through a single cycle of stimulation and expansion. After the last 6 days in IL2-containing medium, cells have been starved from serum for 2h and then the following assays were performed. In (B) the migration index in response to CCL19/CCL21 gradient for 2h has been calculated using transwell migration assay (n=6). In (C) cells have been left to adhere for 30min to fibronectin-coated slides. Then, cells have been stimulated with 50nM CCL19 and 50nM CCL21 chemokines for 15min and then fixed and processed for immunostaining. Representative images showing the mitochondrial network (anti-TOM20 staining) in effector T (Teff) and exhausted T (Tex) cells are shown on the left. Quantification of the percentage of cells showing fragmented mitochondria in each condition is reported in the graph on the right (n=3). In (D) the cells have been stimulated with 50nM CCL19 and 50nM CCL21 chemokines for 15min in an eppendorf tube and then proteins were extracted. The expression level of the indicated (phospho)-proteins has been evaluated by western blot (n=3).
Data are shown as mean ± SEM. Scale bar: 5μm in **C**. Significance is indicated as follows: *=p<0.05; **=p<0.01; ***=p<0.001.